



# Towards higher resolution tomography at the global and regional scales

Lapo Boschi, ETH

Bill Fry, ETH; Daniel Peter, ETH;

— T.W. Becker, USC; G. Ekström, Columbia U., D. Giardini, ETH; B. Steinberger, NGU

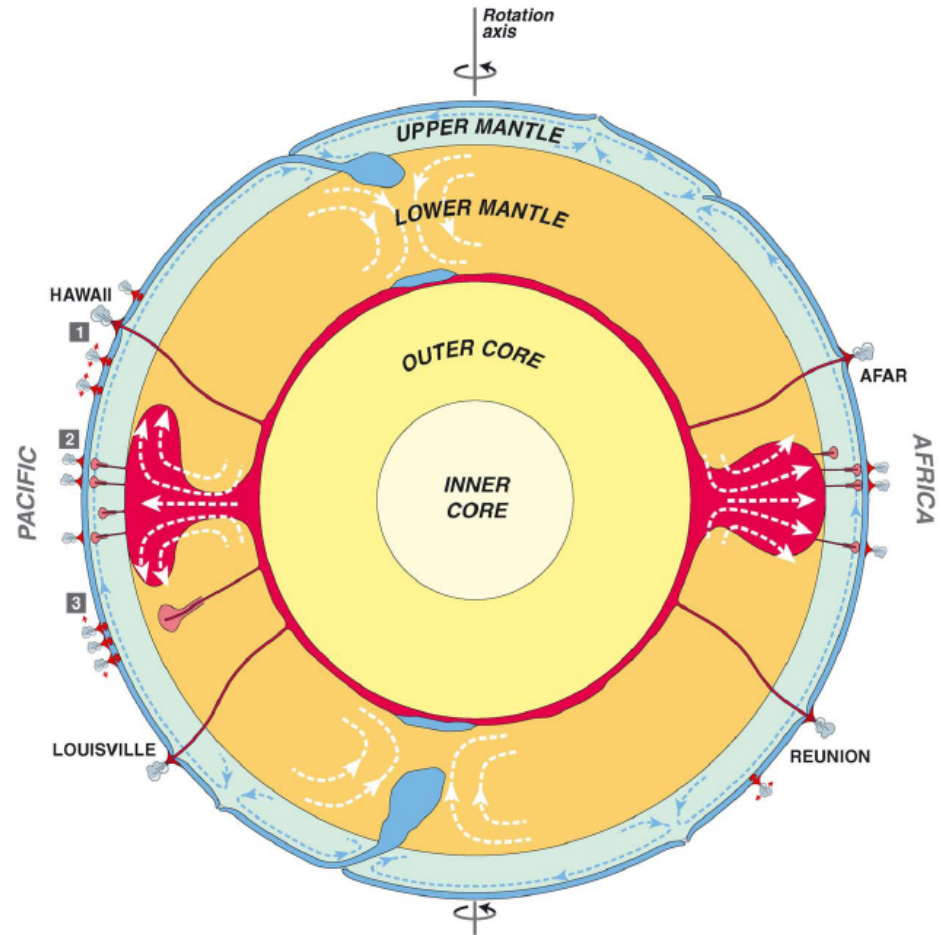


**Do we need higher resolution?**

Thermal plumes rising from an unstable thermal boundary layer in water. The boundary layer has been colored, using an electrochemical technique.

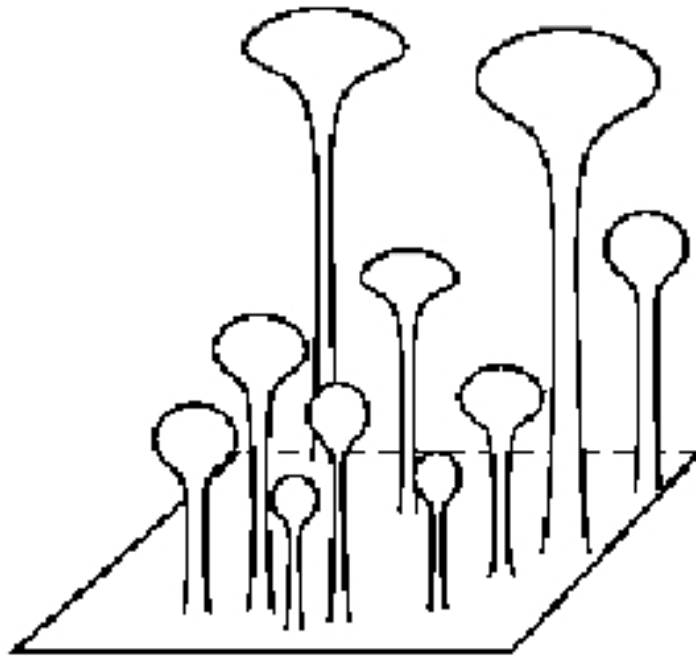
# The origin of hotspots

- Courtillot *et al.* (2003) distinguish hotspots as being caused by
  - i. Deep, narrow plumes
  - ii. Plumes rising from plume-farms at 660
  - iii. “Andersonian” crack-like features

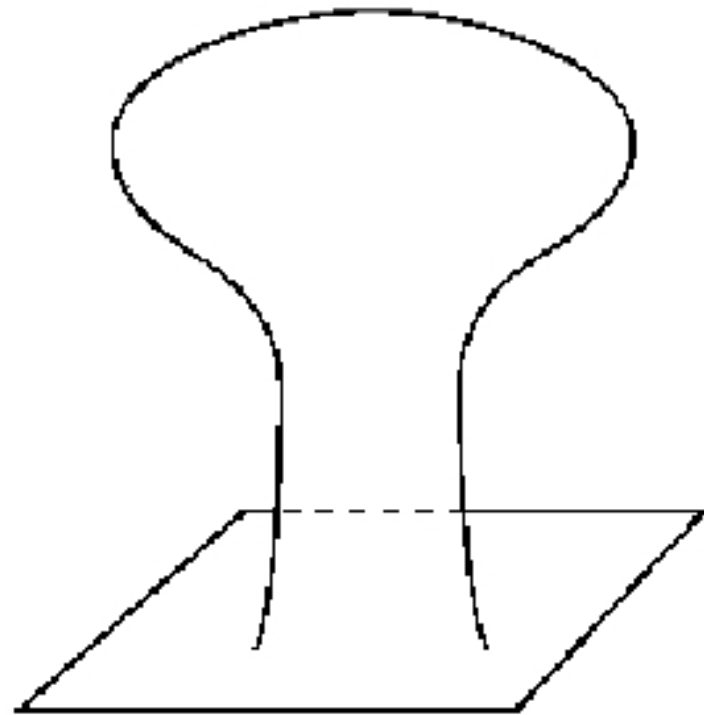


# Schubert et al (2004): Plume clusters

*G. Schubert et al./Physics of the Earth and Planetary Interiors 146 (2004) 147–162*



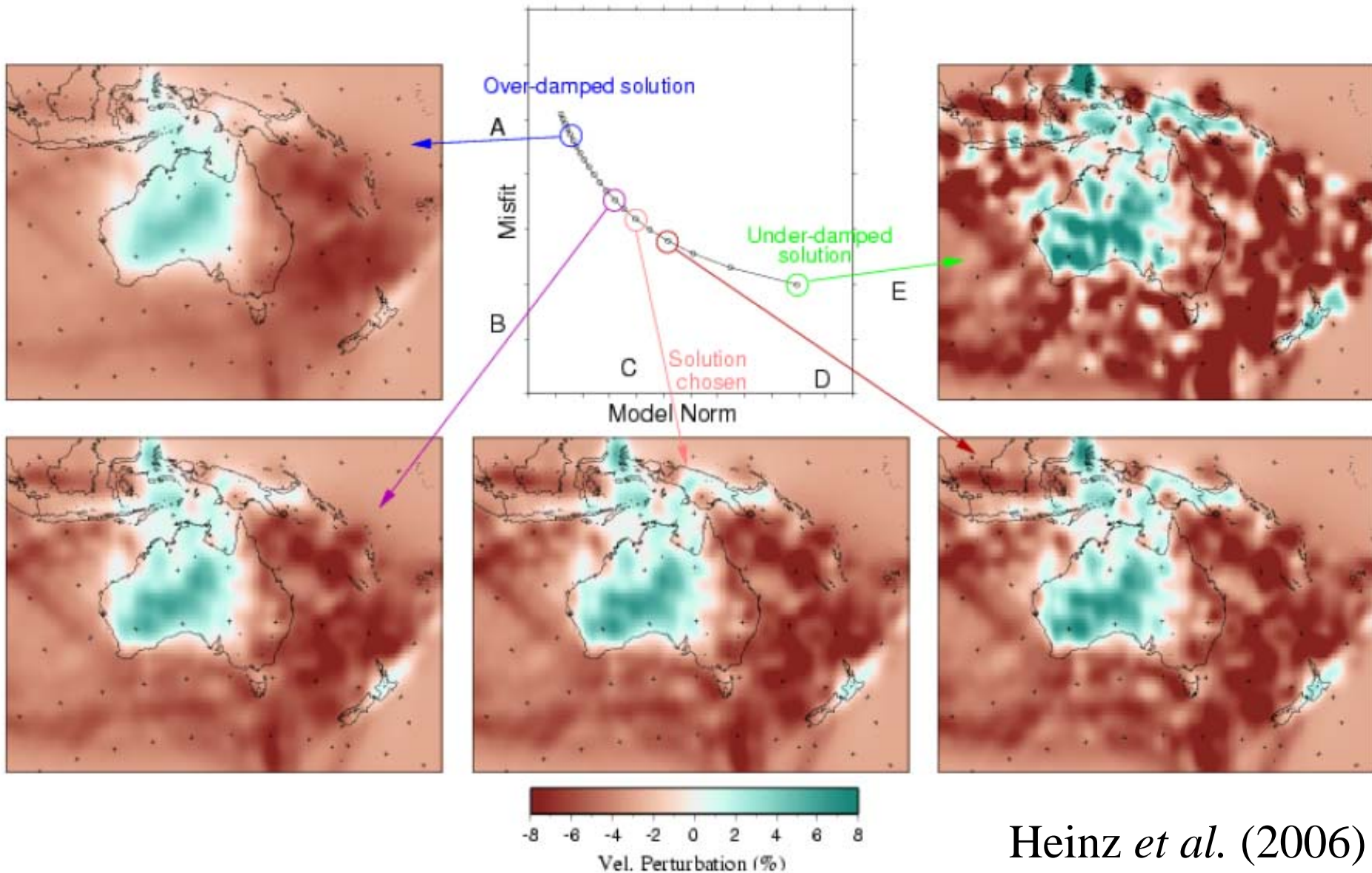
Plume Cluster



Superplume



# Tomography results are non-unique



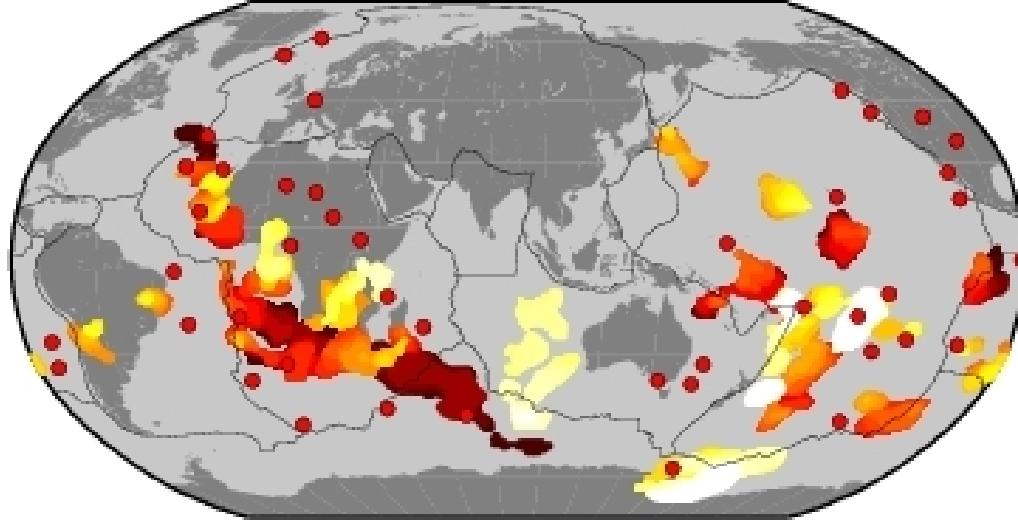
Heinz *et al.* (2006)

# Tomography results are non-unique

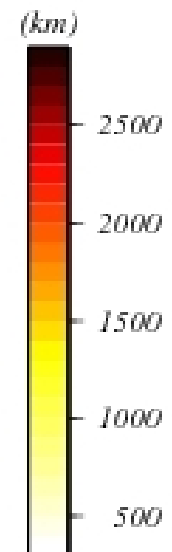
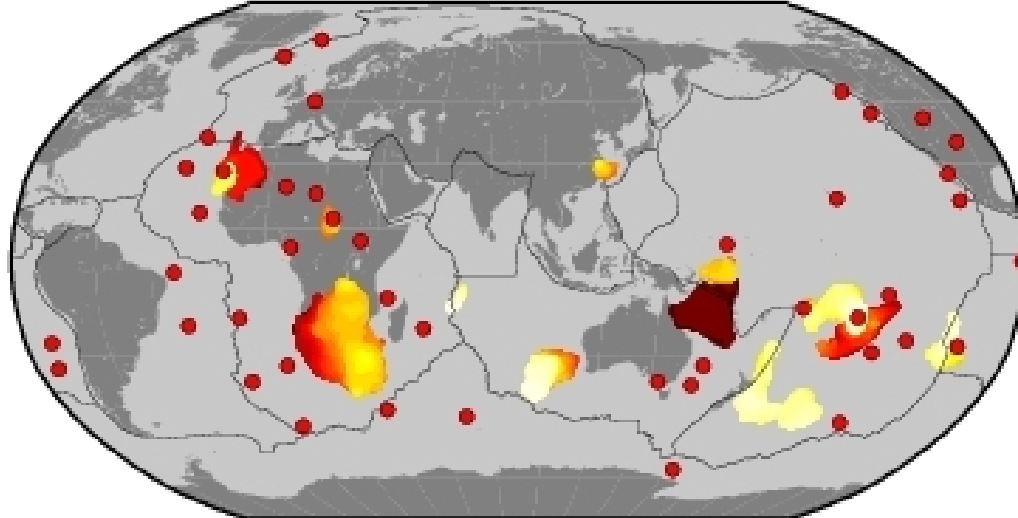
QuickTime™ and a  
Video decompressor  
are needed to see this picture.

# plume detection algorithm applied to two P-wave tomographic models

*vox3p*:  $N_p=46$ ,  $\langle A \rangle=4.40\%$ ,  $\Sigma V=0.83\%$ ,  $\mu=2.50$ ,  $\lambda=0.47$

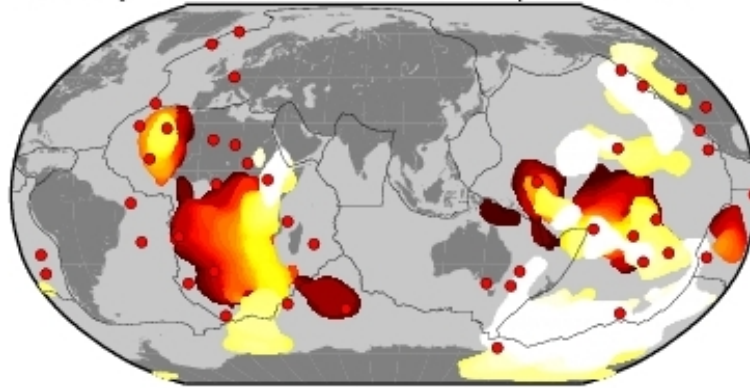


*pri-p05*:  $N_p=26$ ,  $\langle A \rangle=2.73\%$ ,  $\Sigma V=0.52\%$ ,  $\mu=2.87$ ,  $\lambda=0.55$

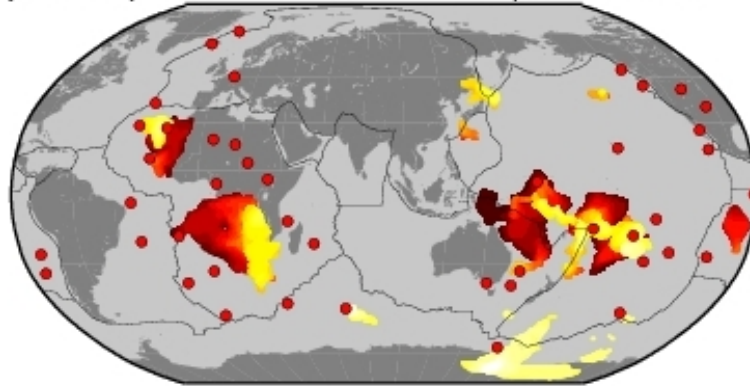


# plume detection algorithm applied to three S-wave models

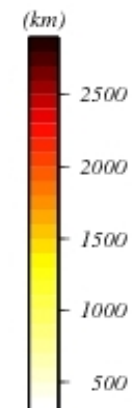
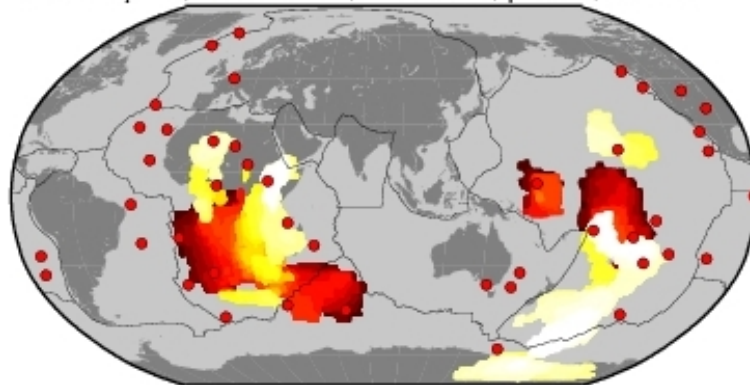
*smean*:  $N_p=18$ ,  $\langle A \rangle=13.37\%$ ,  $\Sigma V=2.86\%$ ,  $\mu=3.36$ ,  $\lambda=0.72$



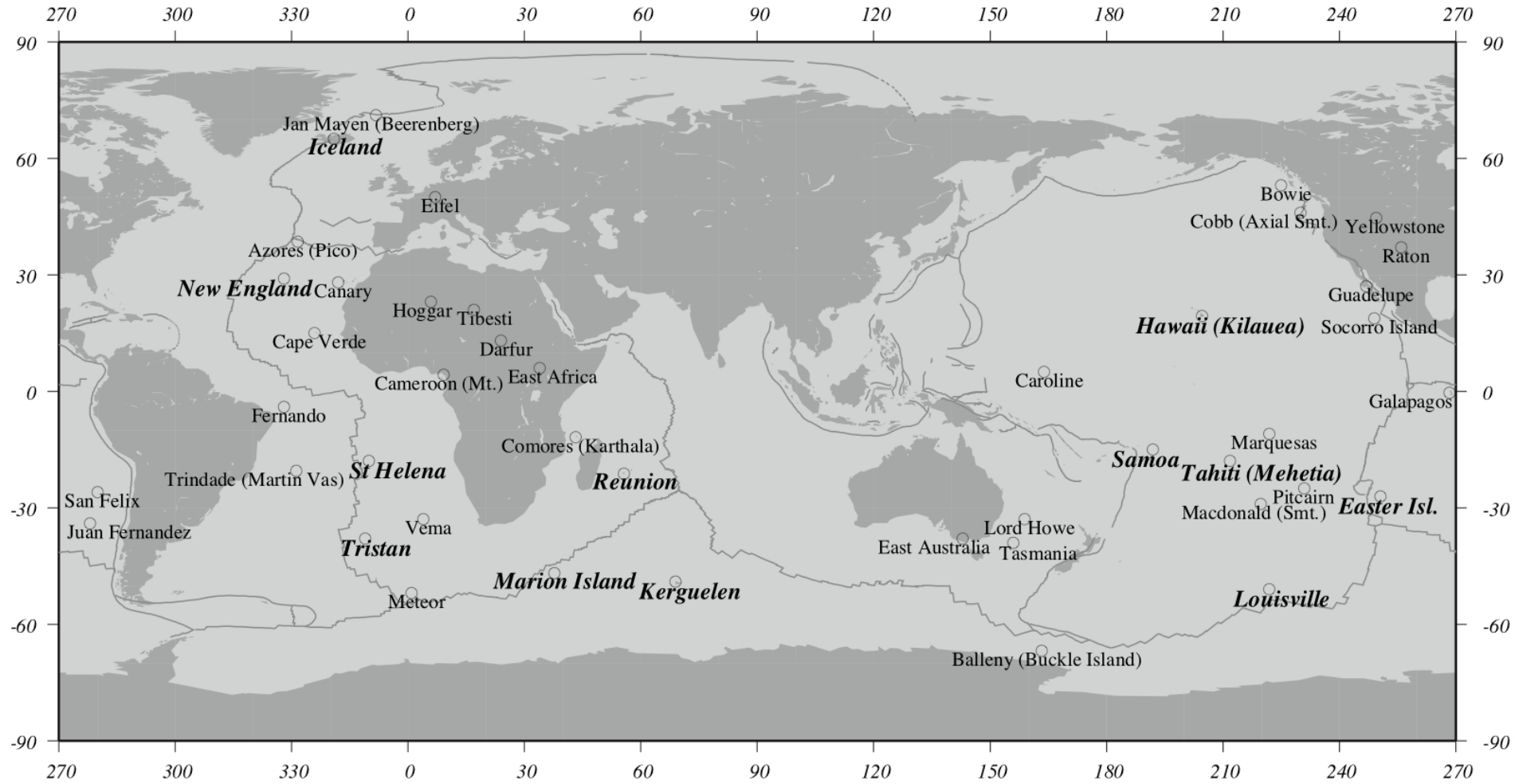
*pri-s05*:  $N_p=29$ ,  $\langle A \rangle=4.08\%$ ,  $\Sigma V=0.61\%$ ,  $\mu=3.96$ ,  $\lambda=0.59$



*tx2007*:  $N_p=14$ ,  $\langle A \rangle=6.60\%$ ,  $\Sigma V=1.29\%$ ,  $\mu=2.89$ ,  $\lambda=0.56$

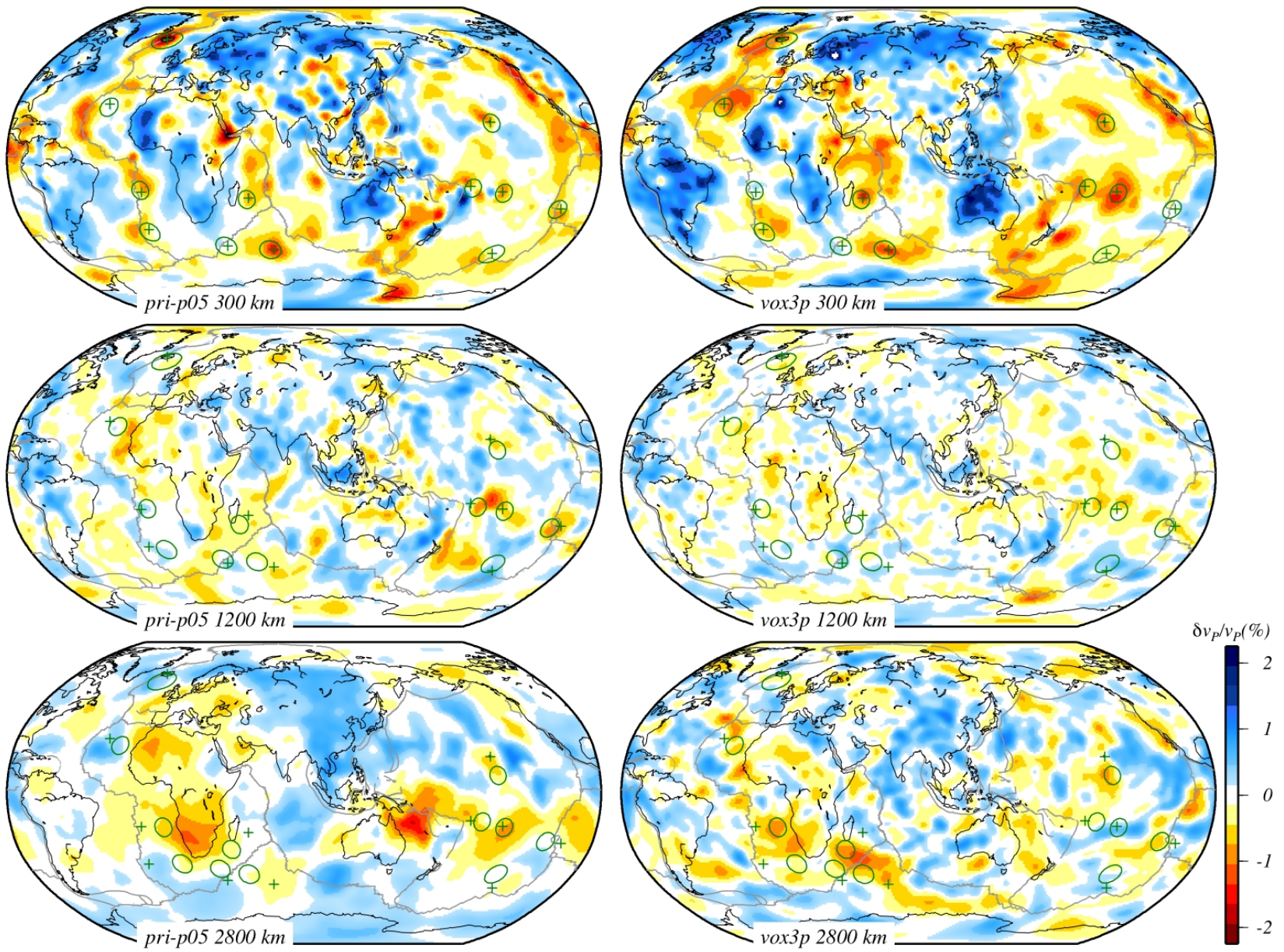


# 44 hotspots that we look at. 12 are suspected to originate from deep upwellings



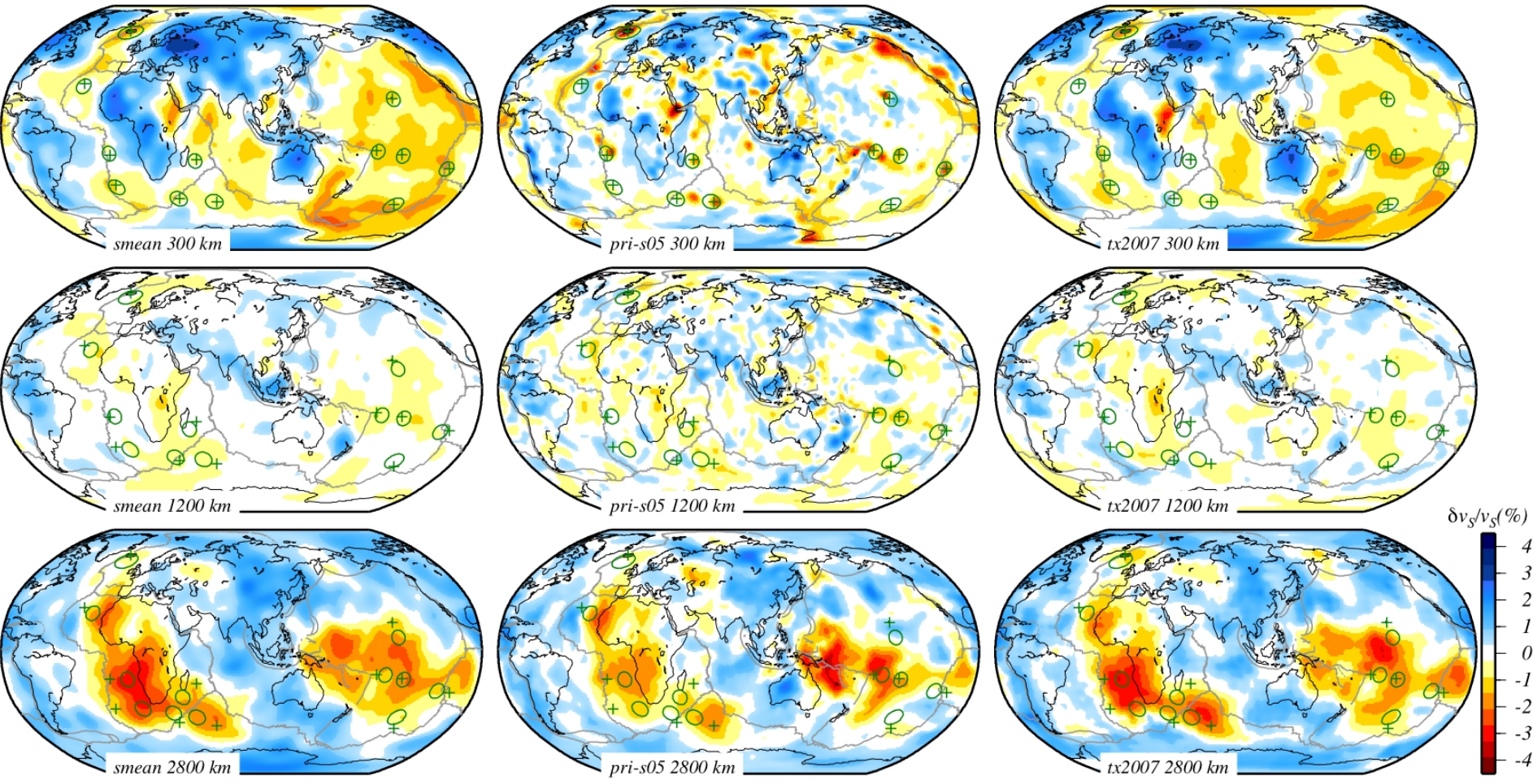


# P tomographic models; 12 likely deep plumes; advection vs. no advection





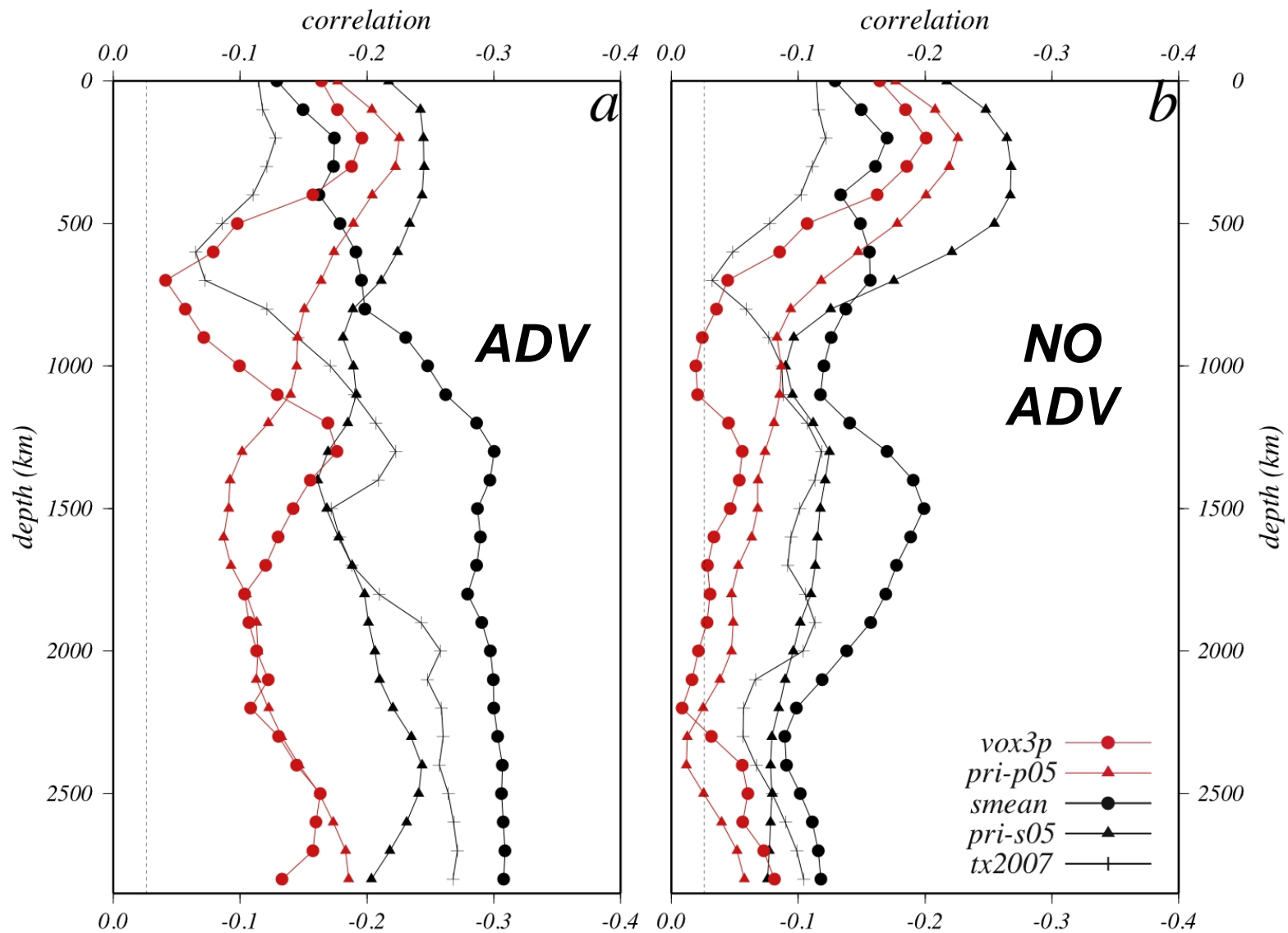
# S tomographic models; 12 likely deep plumes; advection vs. no advection



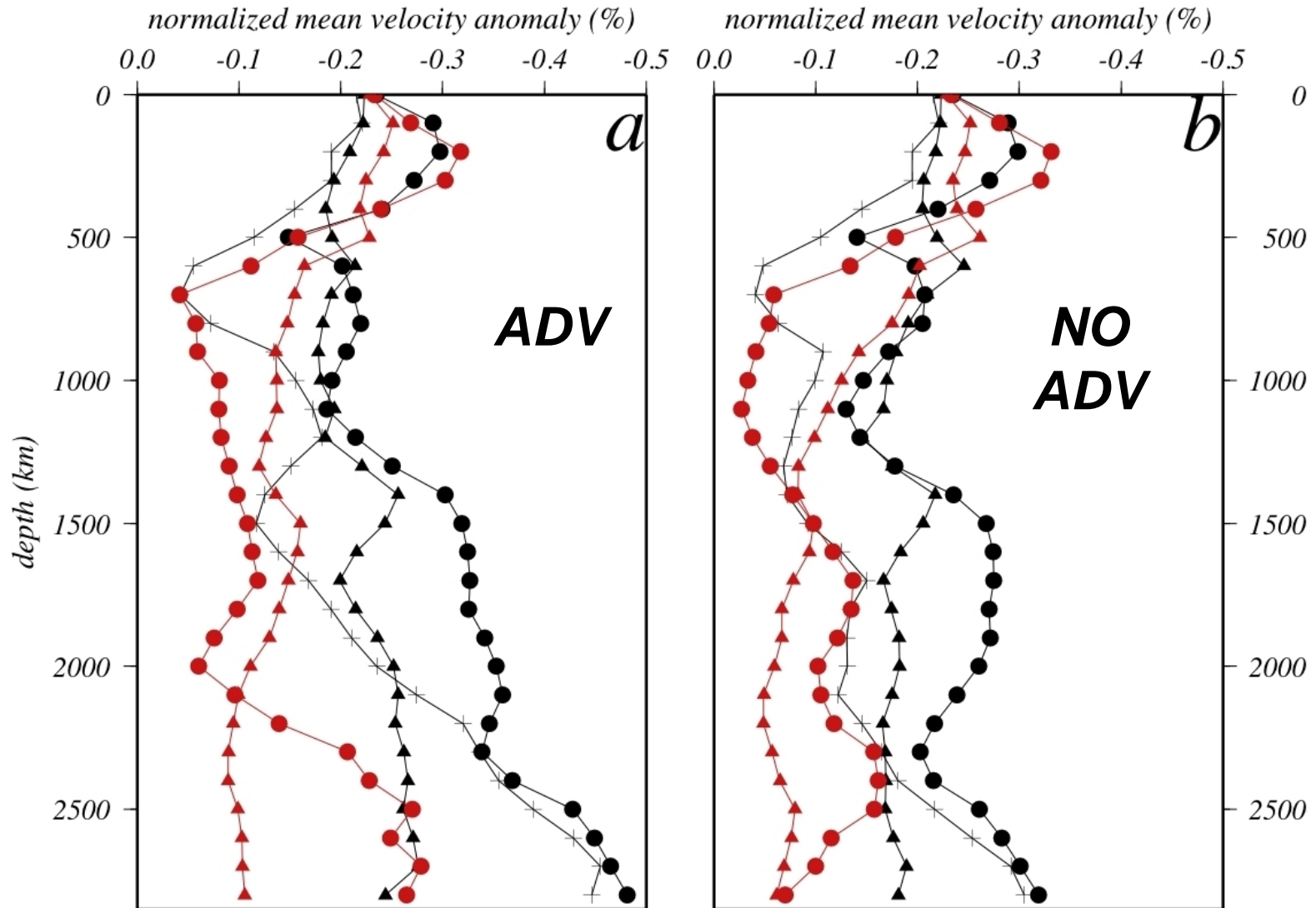


# Are similarities statistically significant?

## correlation



another way of “measuring” plumes in a tomographic model:  
mean velocity anomaly within dynamically modeled plume conduits





A global tomographic map of the Earth's mantle. The map uses a color scale where blue indicates regions of high seismic velocity and red indicates regions of low seismic velocity. A prominent blue feature is visible in the Pacific Ocean region, while a large red feature is seen in the Atlantic and Indian Ocean regions. The map is overlaid with a grid of latitude and longitude lines.

## Answers from tomography

- *some* hotspots can be associated to deep mantle upwellings



## Answers from tomography

- *some* hotspots can be associated to deep mantle upwellings
- With the exception of Iceland, all those hotspots are on top of the Africa and South Pacific low-velocity provinces

## Answers from tomography

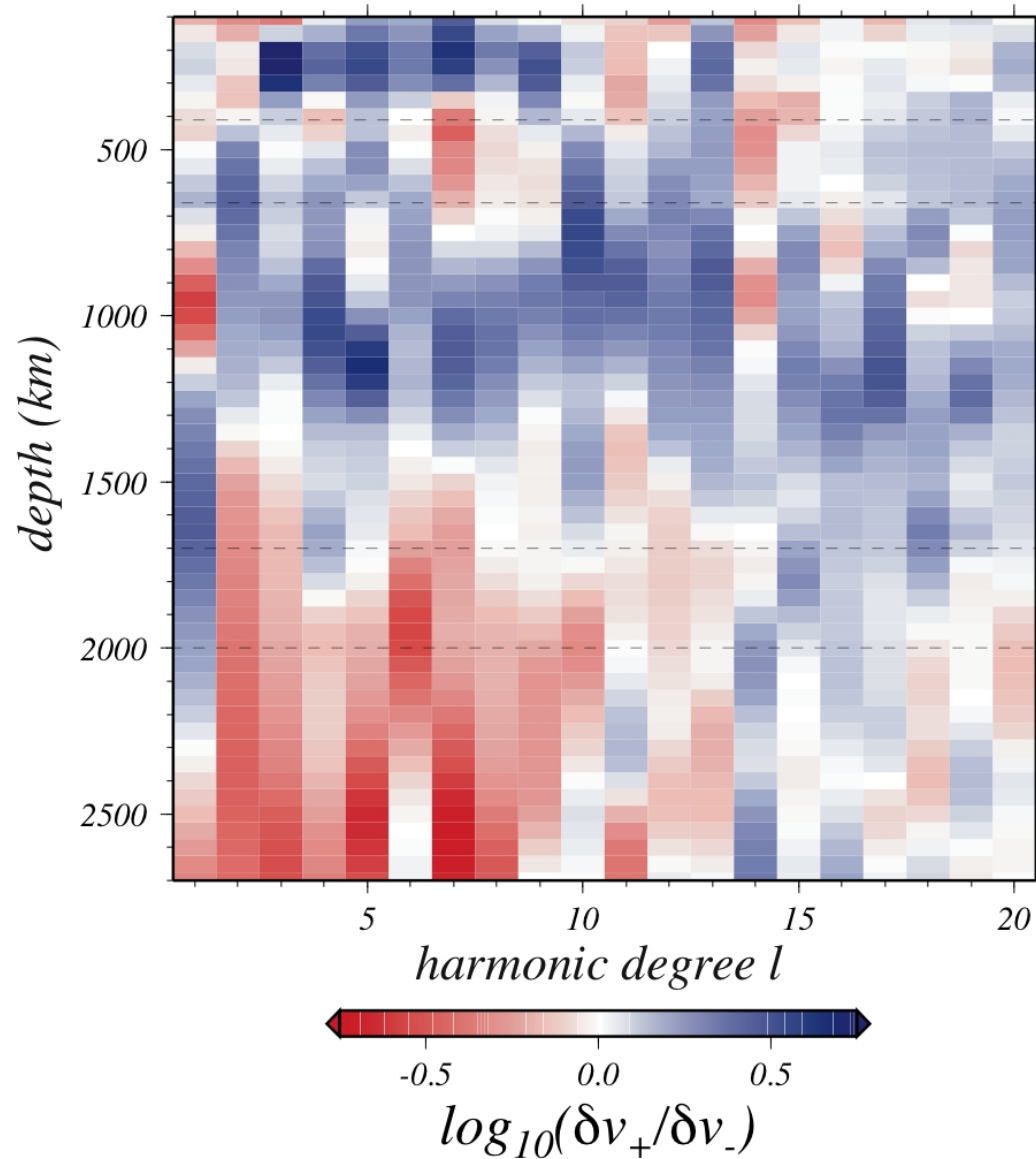
- *some* hotspots can be associated to deep mantle upwellings
- With the exception of Iceland, all those hotspots are on top of the Africa and South Pacific low-velocity provinces
- Hence, superplume-dome and plume-forest models are likely

## Answers from tomography

- *some* hotspots can be associated to deep mantle upwellings
- With the exception of Iceland, all those hotspots are on top of the Africa and South Pacific low-velocity provinces
- Hence, superplume-dome and plume-forest models are likely
- Can we resolve between the two?



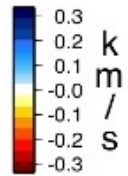
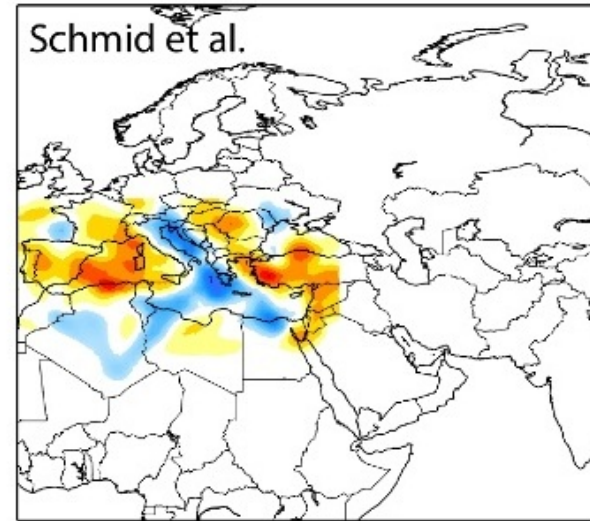
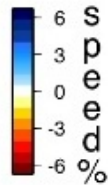
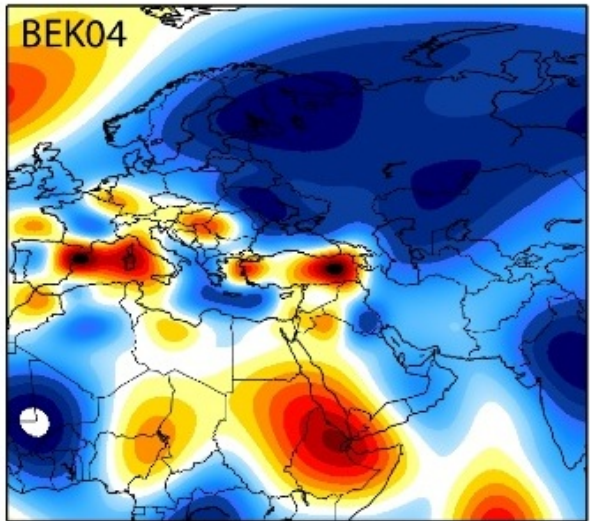
Reif & Williams (2007) compare the spectrum of positive vs. negative velocity anomalies. We apply their analysis to Becker & Boschi's (2002) model smean



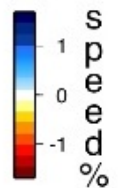
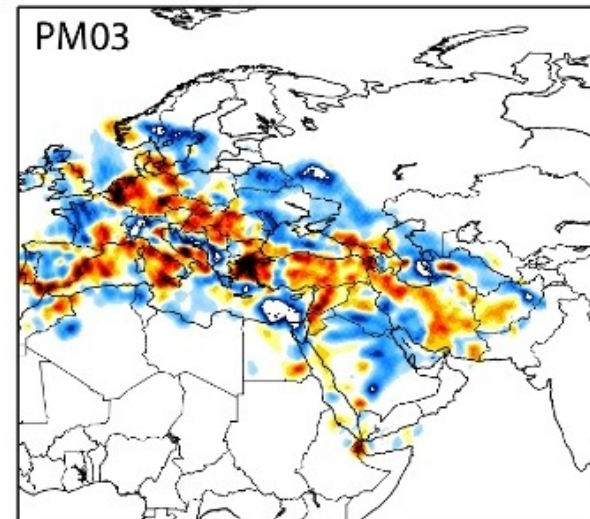
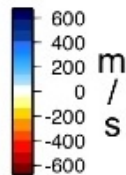
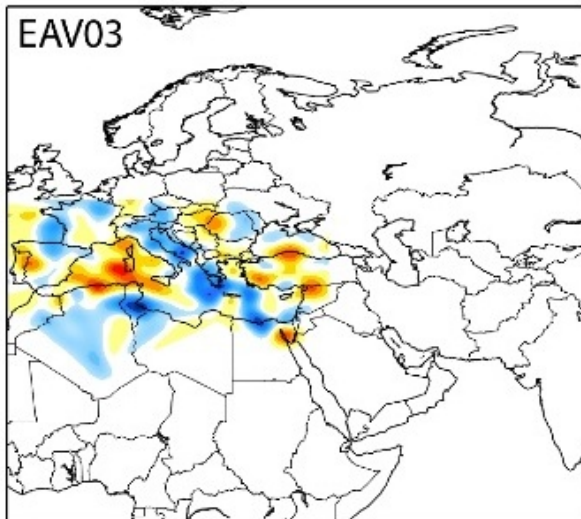
# Plume farms vs plume forests

- Depth dependence of  $dv+/dv-$
- Geographic distribution of hotspots
- detected vertically coherent tomographic anomalies merge at depth
- Significant correlation between modeled plume conduits and tomography
- Icelandic hotspot

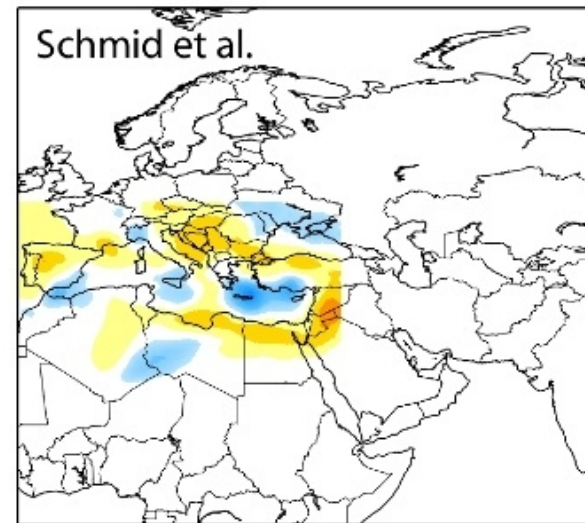
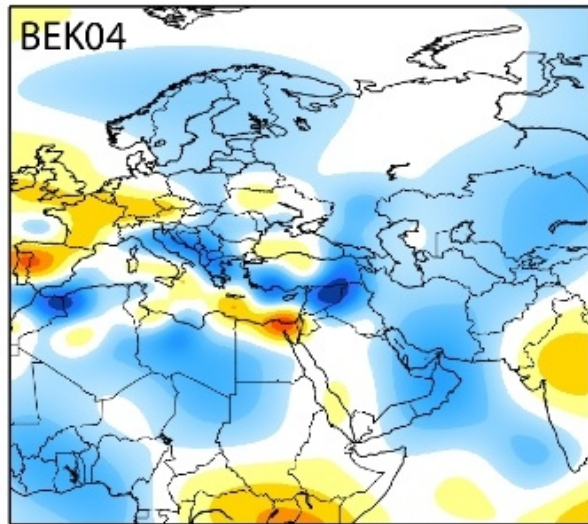
# Local Model “agreement”



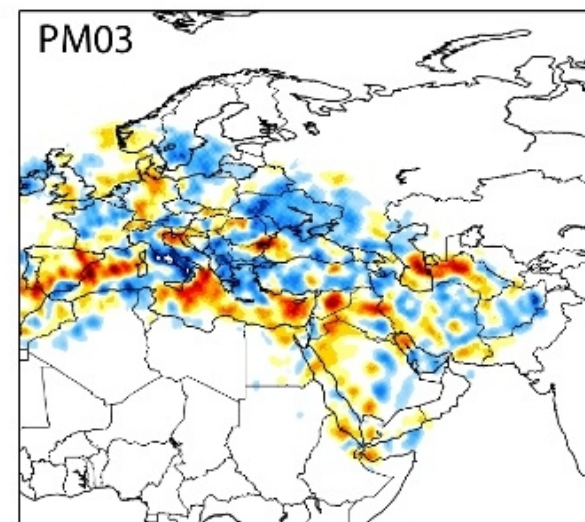
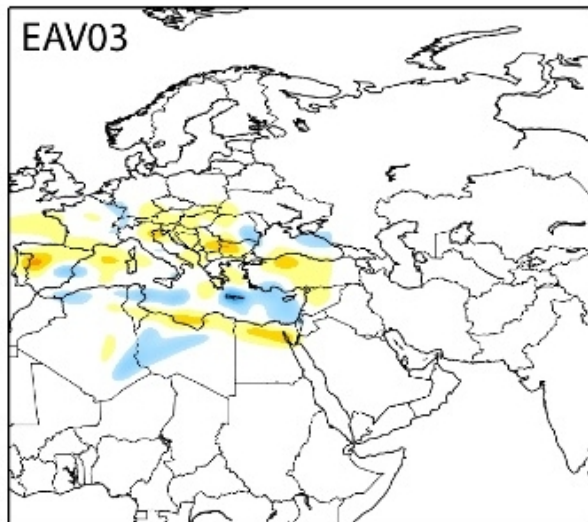
100 km



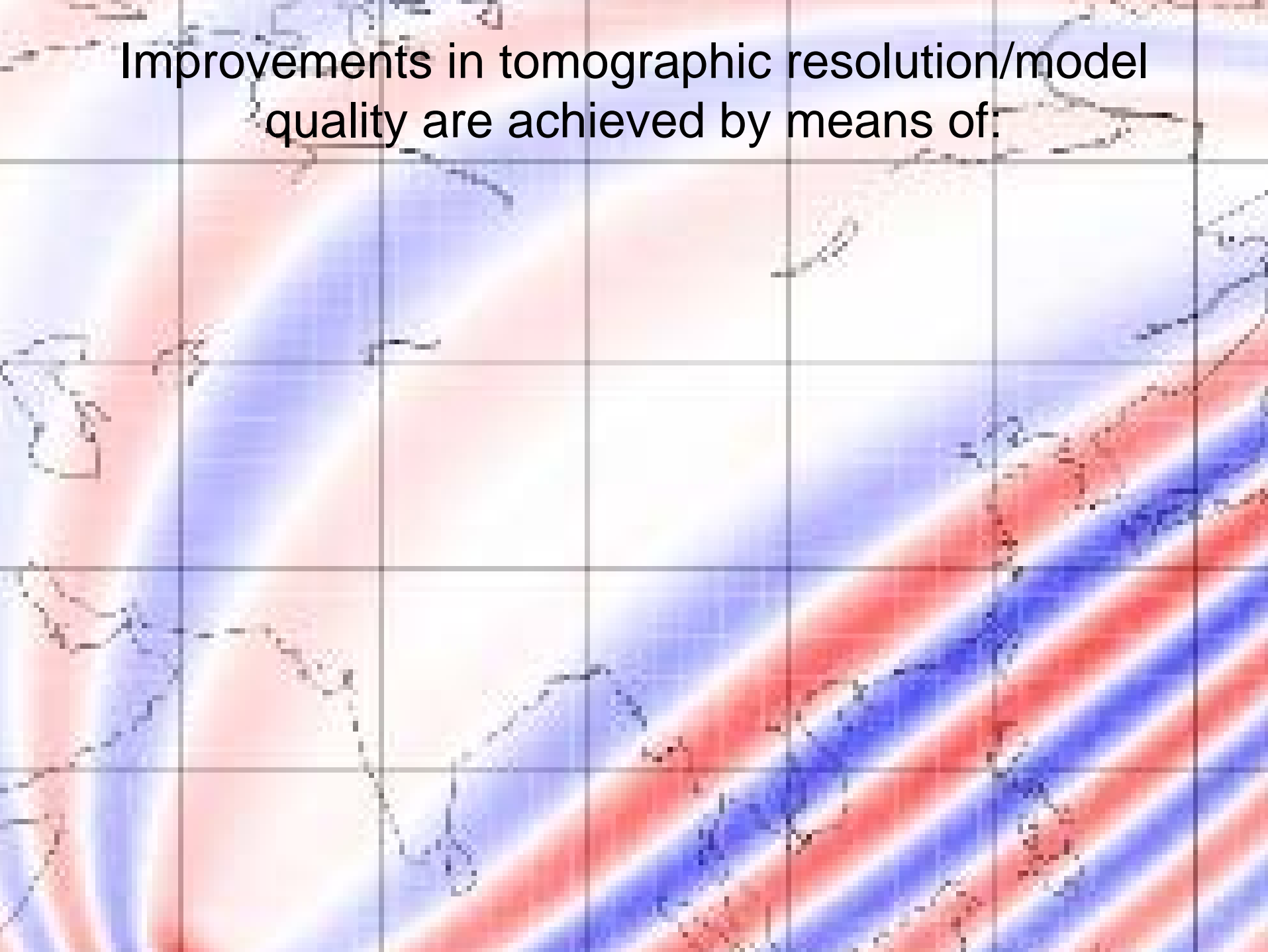
# Local Model “agreement”



300 km



Improvements in tomographic resolution/model quality are achieved by means of:







Improvements in tomographic resolution/model quality are achieved by means of:

- Improvements in data-coverage



Improvements in tomographic resolution/model quality are achieved by means of:

- Improvements in data-coverage
- Improvements in the theoretical formulation of the inverse problem (relation between model and observations)





Improvements in tomographic resolution/model quality are achieved by means of:

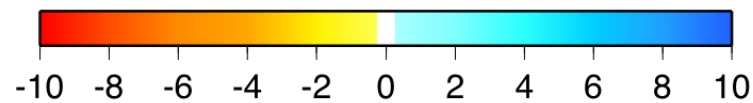
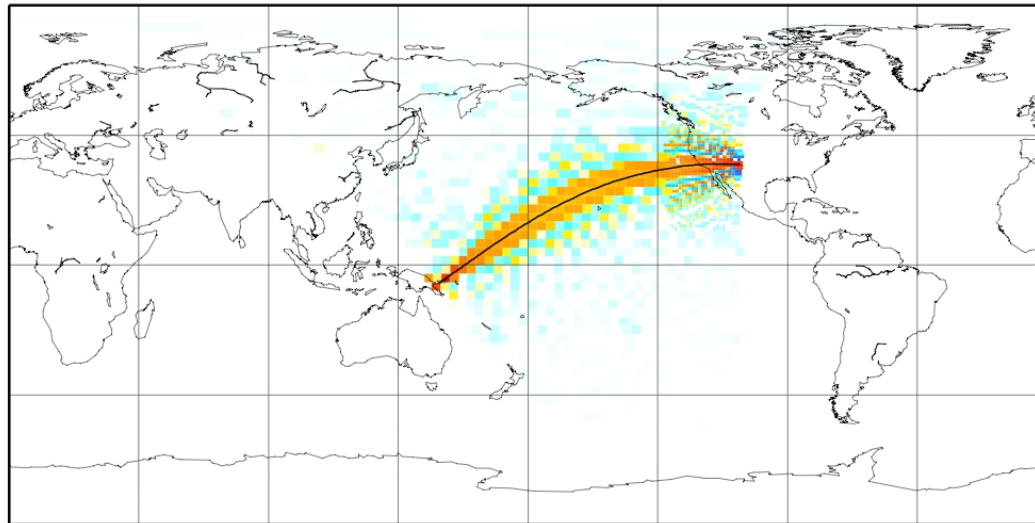
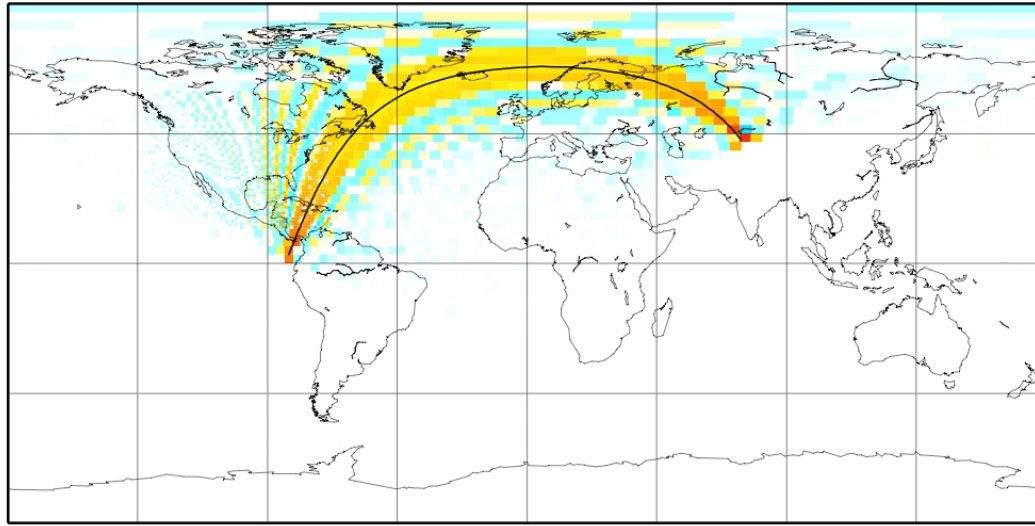
- Improvements in data-coverage
- Improvements in the theoretical formulation of the inverse problem (relation between model and observations)
- Improvements in the accuracy of parameterization and adequacy of regularization scheme

Improvements in tomographic resolution/model quality are achieved by means of:

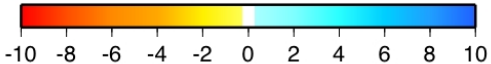
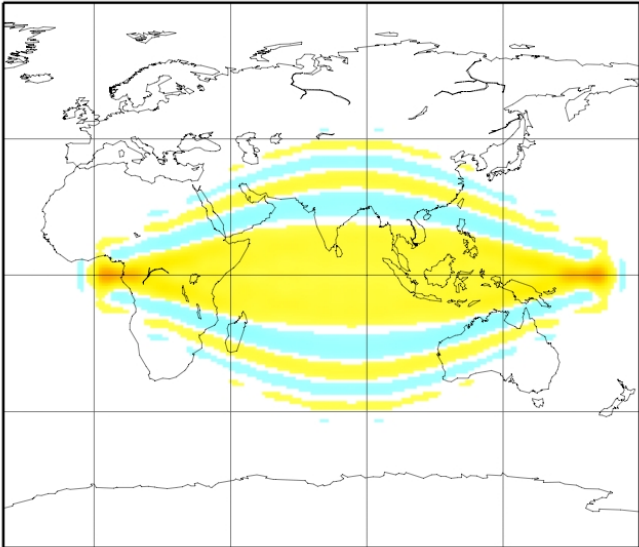
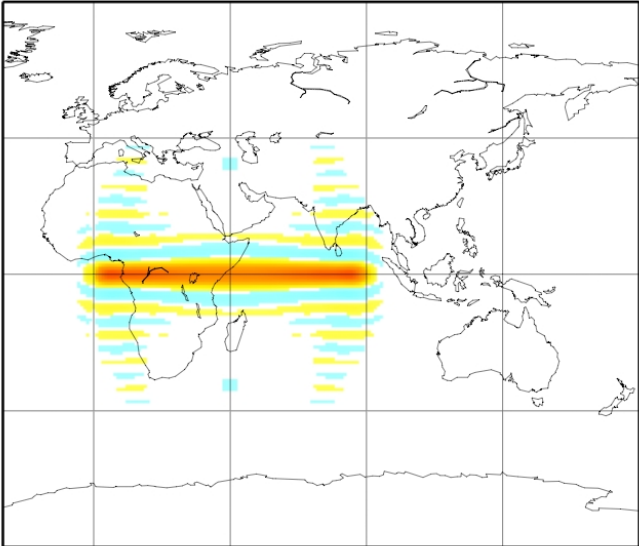
- Improvements in data-coverage
- Improvements in the theoretical formulation of the inverse problem (relation between model and observations)
- Improvements in the accuracy of parameterization and adequacy of regularization scheme

these factors are all coupled with each other

from ray theory to finite frequency theory, and from uniform to multi-resolution parameterization



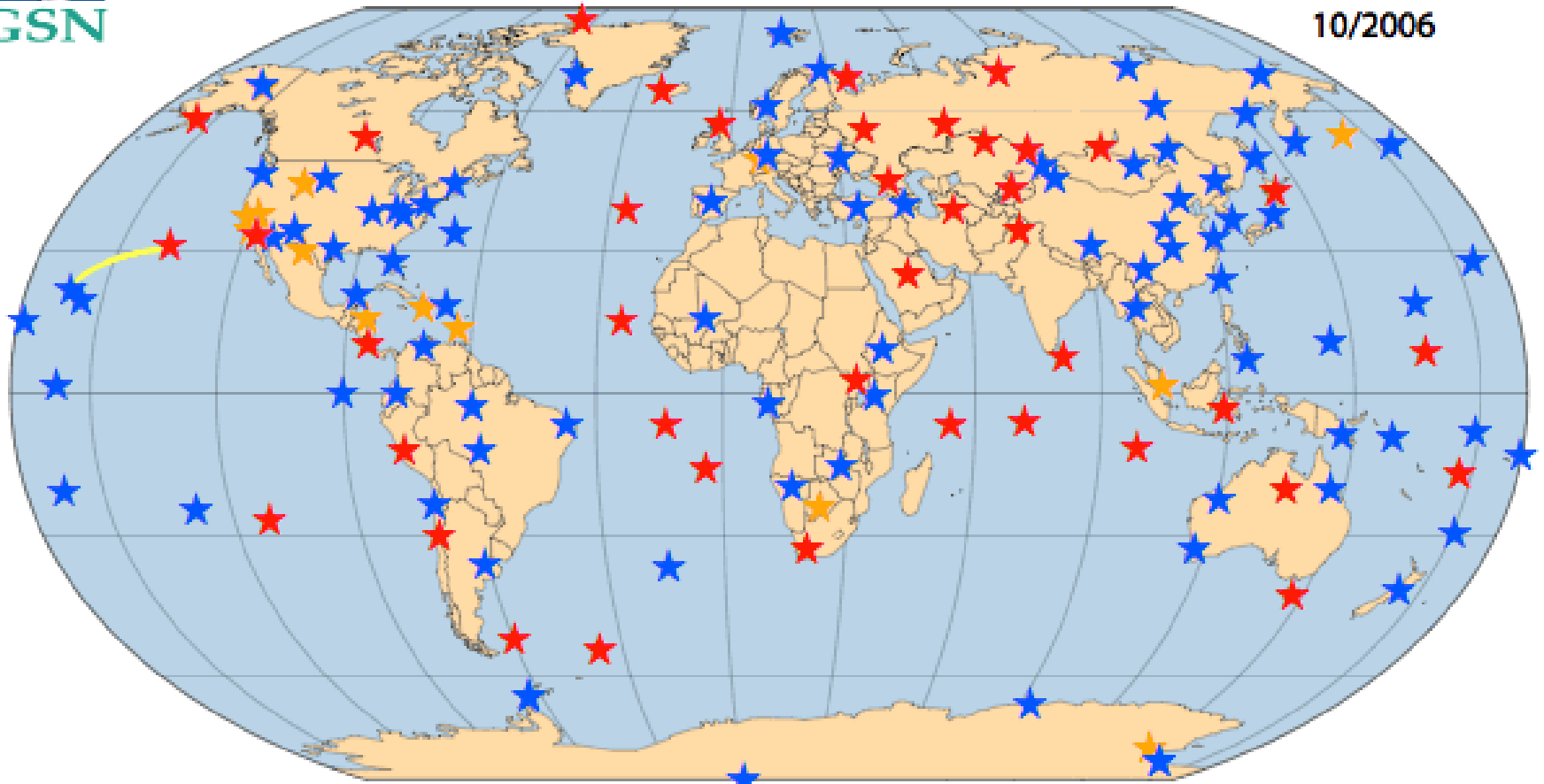
# Uniform resolution parameterization: degree 40 harmonics





# GLOBAL SEISMOGRAPHIC NETWORK

10/2006



★ IRIS / NSF Stations

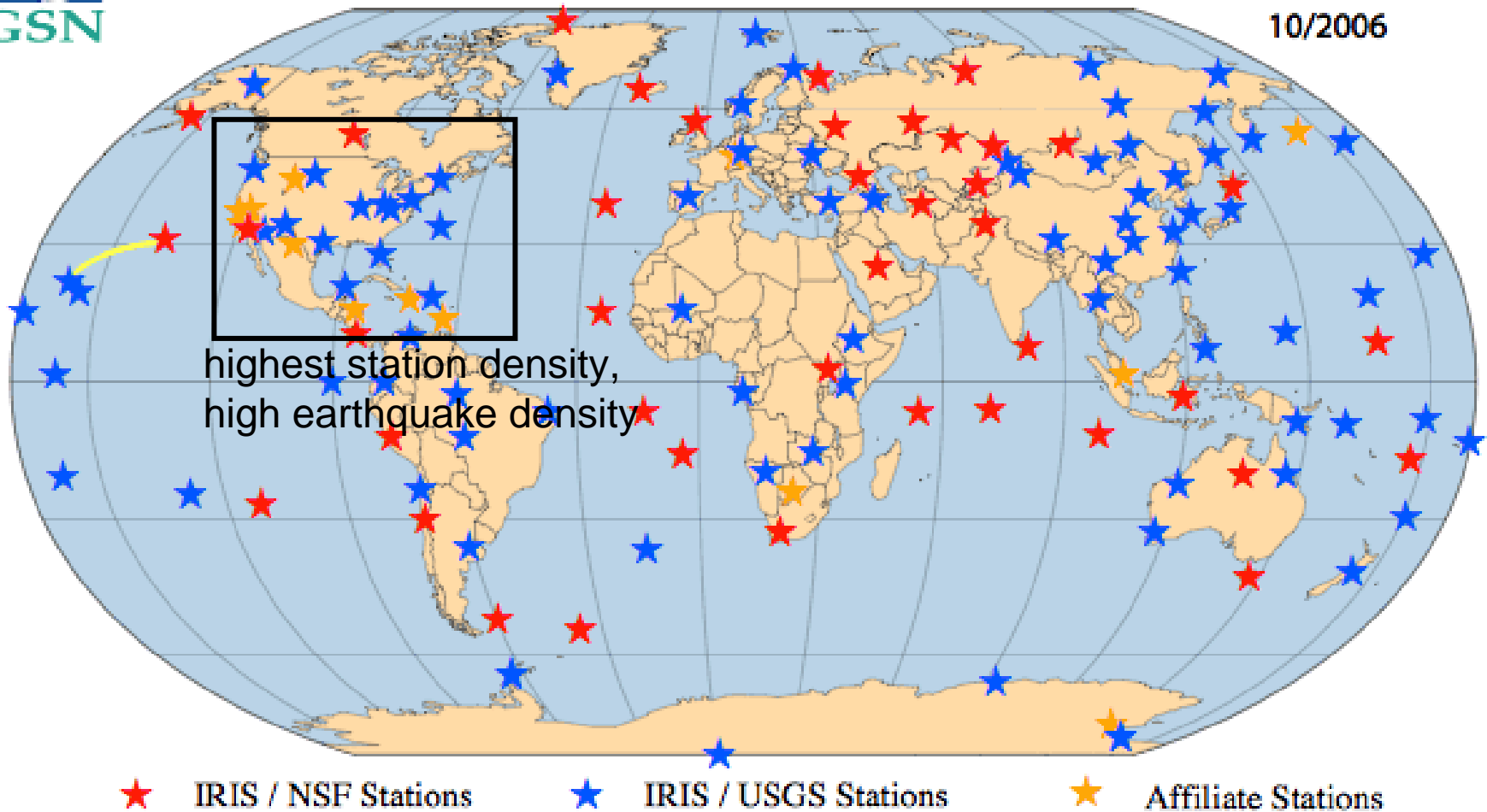
★ IRIS / USGS Stations

★ Affiliate Stations

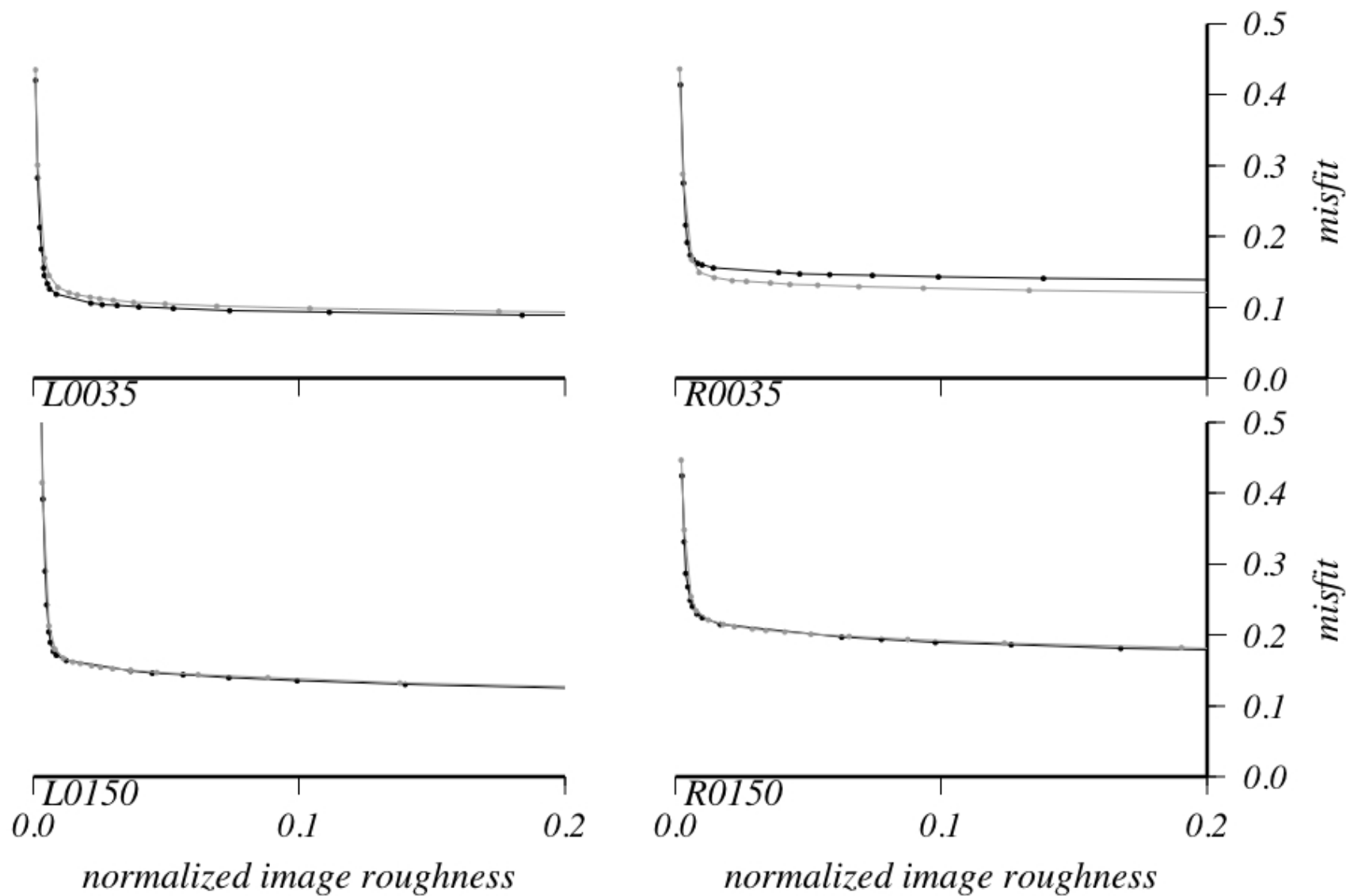


# GLOBAL SEISMOGRAPHIC NETWORK

10/2006



# ray- vs. finite-frequency-theory: trade-off (L-curve) analysis





RAY

Love 150s

BORN

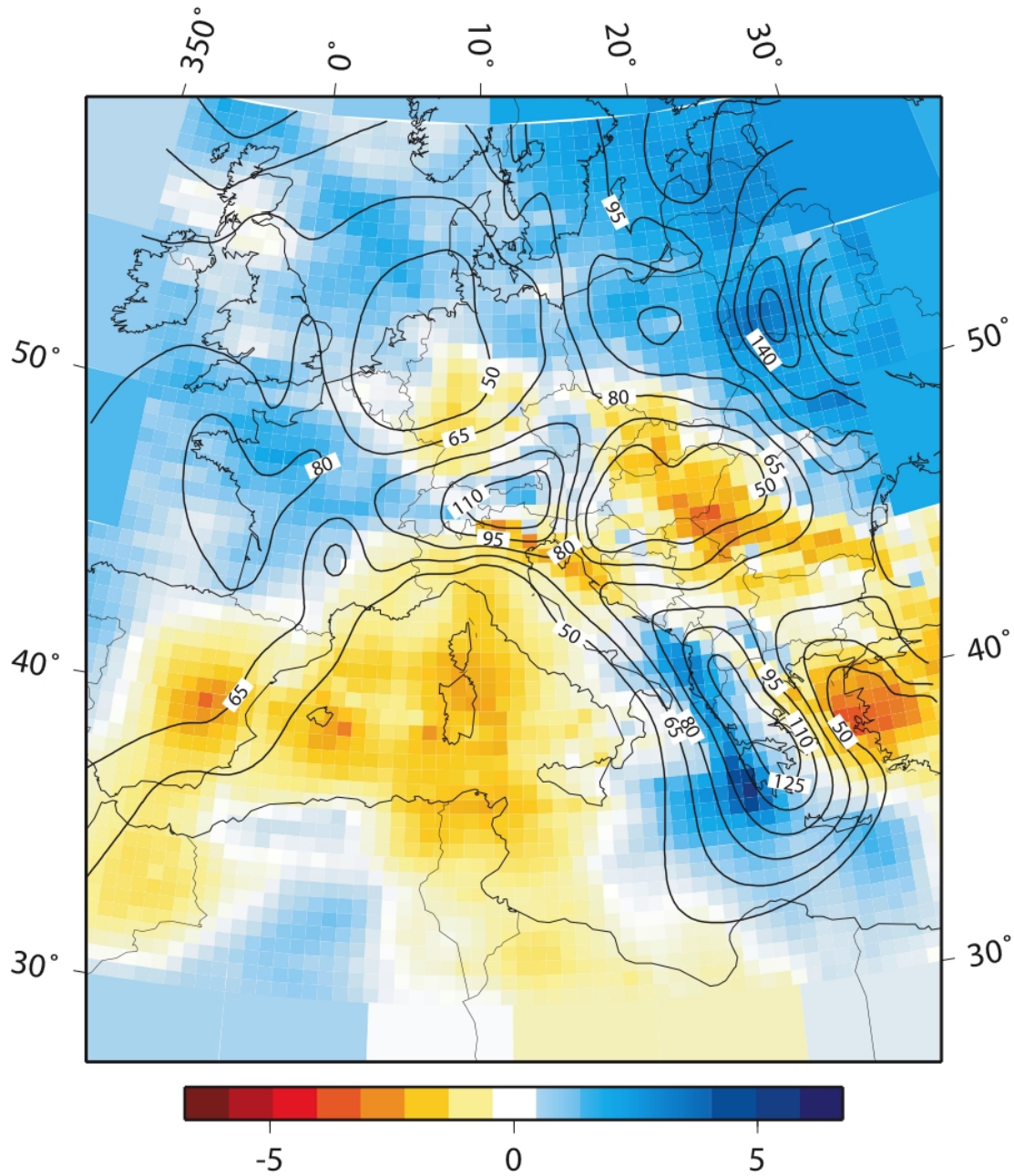
QuickTime™ and a  
Video decompressor  
are needed to see this picture.

QuickTime™ and a  
Video decompressor  
are needed to see this picture.

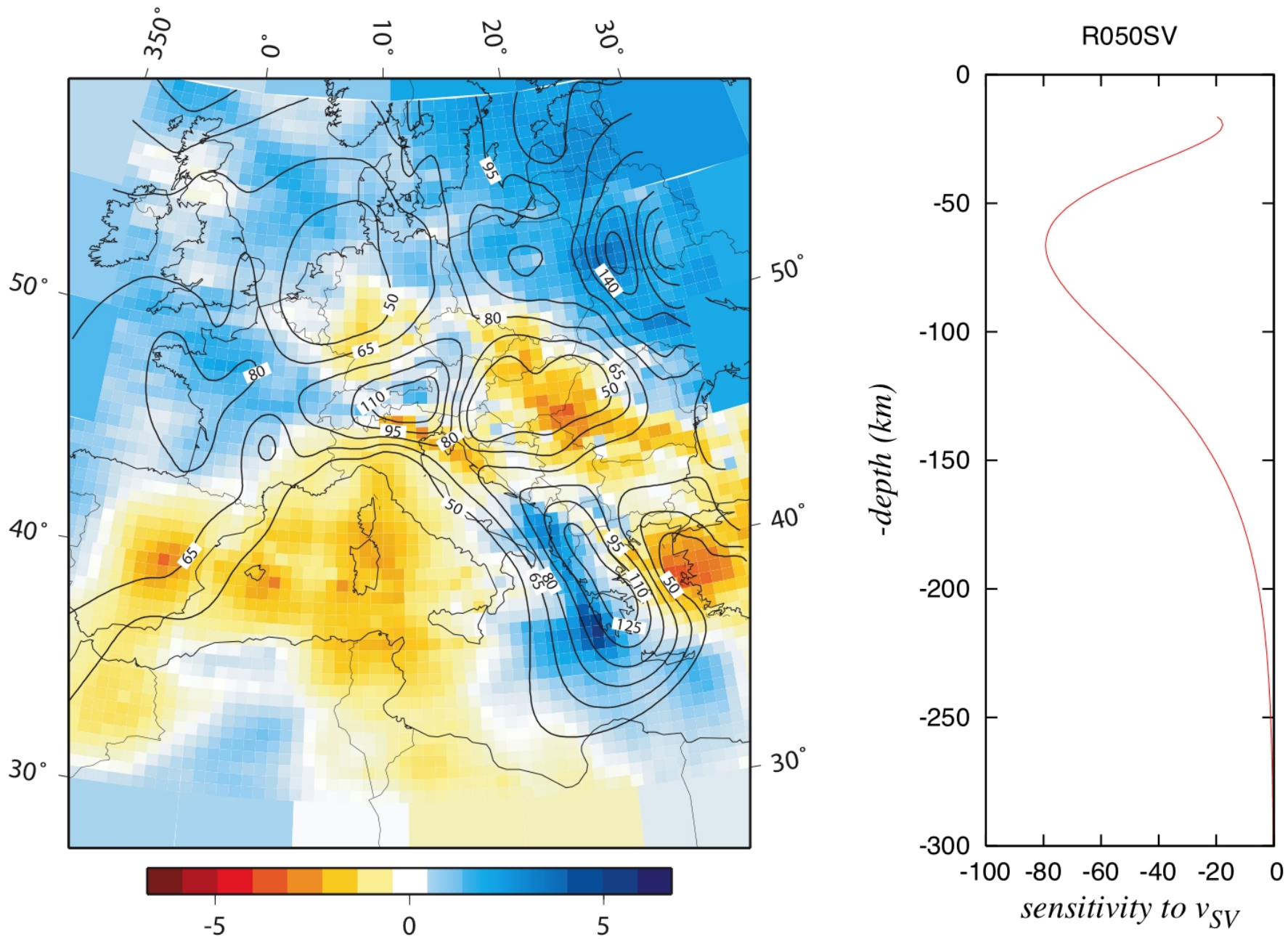
# Improving coverage of the European/mediterranean region



# 50s Rayleigh phase-speed, and depth to 900°C isotherm

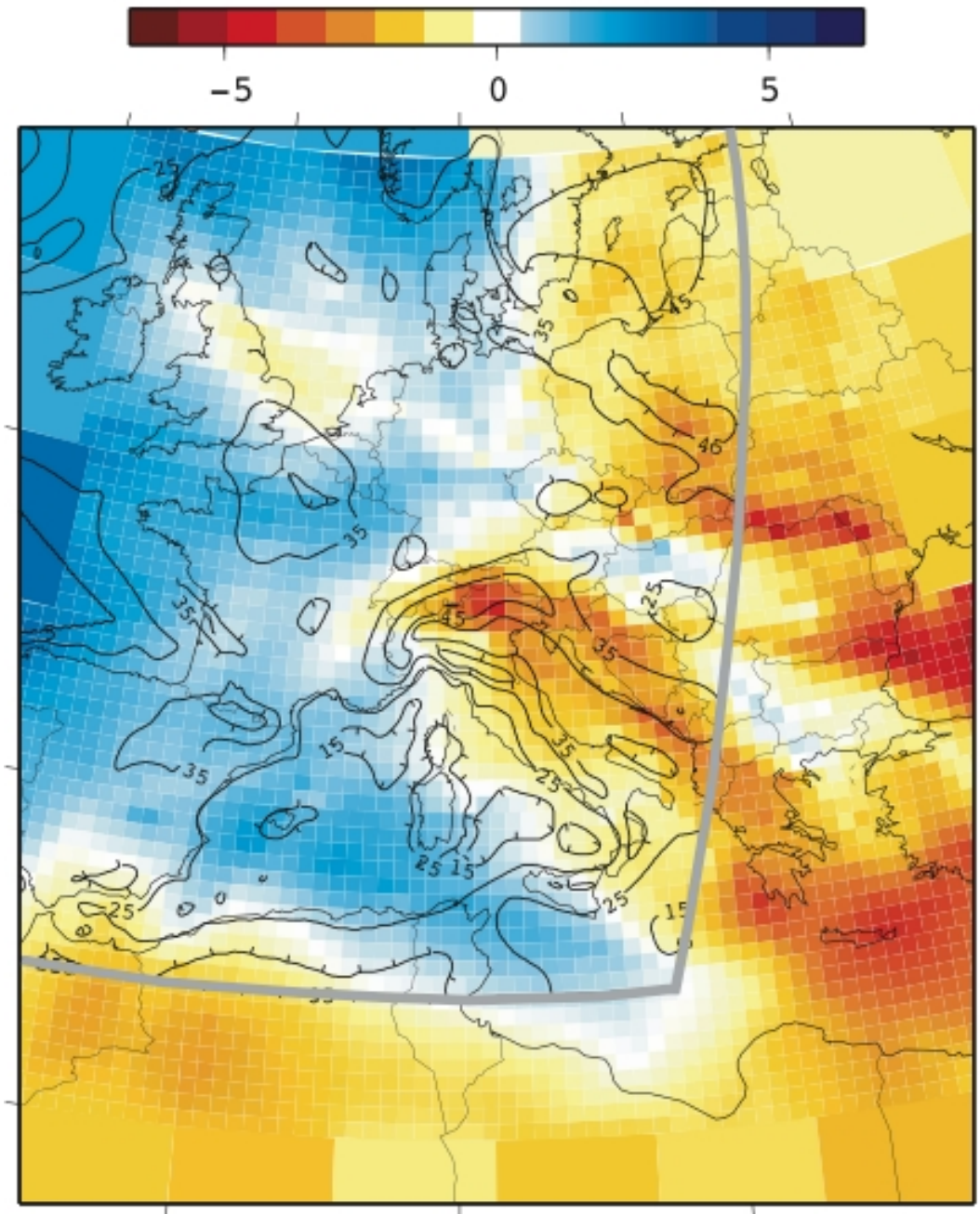


# 50s Rayleigh phase-speed, and depth to 900°C isotherm





35s Love and Moho depth



RAY

L35

BORN

QuickTime™ and a  
Video decompressor  
are needed to see this picture.

QuickTime™ and a  
Video decompressor  
are needed to see this picture.



RAY

R35

BORN

QuickTime™ and a  
Video decompressor  
are needed to see this picture.

QuickTime™ and a  
Video decompressor  
are needed to see this picture.

RAY

L150

BORN

QuickTime™ and a  
Video decompressor  
are needed to see this picture.

QuickTime™ and a  
Video decompressor  
are needed to see this picture.

RAY

R150

BORN

QuickTime™ and a  
Video decompressor  
are needed to see this picture.

QuickTime™ and a  
Video decompressor  
are needed to see this picture.

# Conclusions

- joint refinement of parameterization and data-coverage improves tomographic resolution of European upper mantle, even in a simple ray-theory formulation.

# Conclusions

- joint refinement of parameterization and data-coverage improves tomographic resolution of European upper mantle, even in a simple ray-theory formulation.
- in our North America experiment (data coverage still not optimal) account of single scattering did not alter tomographic images significantly.

# Conclusions

- joint refinement of parameterization and data-coverage improves tomographic resolution of European upper mantle, even in a simple ray-theory formulation.
- in our North America experiment (data coverage still not optimal) account of single scattering did not alter tomographic images significantly.
- in our Europe experiment, significant single-scattering effects are noted in at least one surface-wave mode. We are not ready yet to prove that this reflects an improvement in image quality.